

Collective Molecular Dynamics in Proteins and Membranes

Maikel C. Rheinstädter*

Department of Physics and Astronomy,

University of Missouri-Columbia, Columbia, MO 65211, U.S.A.

(Dated: October 29, 2018)

Abstract

The understanding of dynamics and functioning of biological membranes and in particular of membrane embedded proteins is one of the most fundamental problems and challenges in modern biology and biophysics. In particular the impact of membrane composition and properties and of structure and dynamics of the surrounding hydration water on protein function is an upcoming hot topic, which can be addressed by modern experimental and computational techniques. Correlated molecular motions might play a crucial role for the understanding of, for instance, transport processes and elastic properties, and might be relevant for protein function. Experimentally that involves determining dispersion relations for the different molecular components, i.e., the length scale dependent excitation frequencies and relaxation rates. Only very few experimental techniques can access dynamical properties in biological materials on the nanometer scale, and resolve dynamics of lipid molecules, hydration water molecules and proteins and the interaction between them. In this context, inelastic neutron scattering turned out to be a very powerful tool to study dynamics and interactions in biomolecular materials up to relevant nanosecond time scales and down to the nanometer length scale. We review and discuss inelastic neutron scattering experiments to study membrane elasticity and protein-protein interactions of membrane embedded proteins.

*Electronic address: RheinstadterM@missouri.edu

I. INTRODUCTION

Dynamics in biological membranes occur on a wide range of length and time scales and involves interactions between the different constituents, such as lipids, cholesterol, peptides and proteins, as sketched in Figure 1. Often, the structure of these systems is relatively well known and the corresponding experimental techniques, such as x-ray crystallography, Nuclear Magnetic Resonance (NMR), and also Atomic Force Microscopy (AFM) have developed standard techniques in many disciplines. The access to dynamical properties turned out to be more difficult. Dynamical properties are often less well understood in biomolecular systems, but are important for many fundamental biomaterial properties such as, e.g., elasticity properties and interaction forces, and might determine or strongly affect certain functional aspects, such as diffusion and parallel and perpendicular transport through a bilayer, and also protein function. New developments and improvements in neutron scattering instrumentation, sample preparation and environments and, eventually, the more and more powerful neutron sources open up the possibility to study collective molecular motions on lateral length scales between micrometers down to a few Angstroms (\AA). The fluctuations are quantified by measuring the corresponding dispersion relations, i.e., the wave vector-dependence of the excitation frequencies or relaxation rates. Because biological materials lack an overall crystal structure, in order to fully characterize the fluctuations and to compare experimental results with membrane theories, the measurements must cover a very large range of length and time scales [1]. The combination of various inelastic scattering techniques, such as inelastic neutron and x-ray scattering, and dynamic light scattering, enlarges the window of accessible momentum and energy transfers - or better: accessible length and time scales - and allows one to study structure and dynamics from the nearest-neighbor distances of lipid molecules to more than 100 nanometers (three orders of magnitude), covering time scales from about one tenth of a picoseconds to almost 1 second (twelve orders of magnitude). The spectrum of fluctuations in model membranes for example covers the long wavelength undulation and bending modes of the bilayer with typical relaxation times of nanoseconds and lateral length scales of several hundred lipid molecules, down to the short-wavelength, picosecond density fluctuations involving neighboring lipid molecules.

Even that membranes are now studied extensively for more than three decades [2], the field is currently boosted by the inter disciplinary interest in life sciences. New and more

powerful techniques might give a quantitative access to molecular properties of the bilayers. Often, phospholipid bilayers are used as model systems to study fundamental properties [3, 4, 5]. But the trend definitely goes to more complex and relevant systems, decorated with cholesterol, peptides and proteins to eventually develop a better understanding of biological membranes. Different model systems are used in experiments and Molecular Dynamics Simulations (MD). In scattering experiments, the weak signals arising from dynamical modes can be multiplexed by using stacked membrane systems and large system sizes, i.e., membrane patches in the order of micrometers and larger. The advantage is the large sampling rate, which makes very small signals visible, and the large ensemble average, which averages over defects. The 'multi-scale' character of biological membranes, i.e., that relevant dynamics occur on a large range of length and time scales [6, 7, 8], poses particular problems because different techniques and probes must be applied to access the different lengths and frequencies. Scattering techniques are particularly powerful in spatially ordered systems and have been very successfully applied to study structure and dynamics (phonons) in crystals. In soft-matter and biology, a periodic structure is often missing or not well developed and new concepts and approaches are required to study structural and dynamical properties. In contrast to computer simulations, where different molecular components and dynamics can well be extracted and distinguished, in experiments there usually is a superposition of signals of different molecular components and interactions, and also single-molecule and collective dynamics. By using different sample geometries, these signals might be separated by their position in reciprocal and frequency space. Selective deuteration is used to distinguish between incoherent and coherent dynamics. Because of more and more powerful spectrometers, smaller and smaller system dimensions and less and less material can be used in experiments. But experiments are still orders of magnitude away from single molecule spectroscopy of, e.g., membrane embedded proteins, which might be envisioned in the next decade.

Even that computer power and access to powerful clusters has drastically increased in the last couple of years, MD simulations are still limited when it comes to large system sizes. Standard membrane systems are single bilayers, and contain several hundred lipid molecules, leading to patch sizes of about 100 Å, and equilibrated for about 100 nanoseconds [9, 10]. The system size, D , produces a cut off wavelength ($\lambda = 2\pi/D$) for the dynamical modes that can be observed and quantified. To properly determine an excitation frequency or

relaxation rate from the time evolution of the scattering functions, the simulations must cover at least two orders of magnitude more in maximal accessible time, thereby limiting the accessible frequencies to about 1 ns. So simulations are still very much limited to fast short wavelength dynamics. When (single) proteins are simulated, the small system size prevents to study the influence of bilayer dynamics to protein dynamics and function, and also a possible protein-protein interaction, which might be relevant for biological function. Analytical theory for membranes is usually based on the theory developed for liquid crystals [11, 12, 13]. It is challenging how microscopic properties, such as the lipid composition of a bilayer, affects macroscopic behavior. However, theories are very important to determine properties from fitting experimental and computational data.

Collective molecular motions impact, e.g., on properties and functionalities of artificial and biological membranes, such as elasticity, transport processes, and inter-protein interaction. Two examples will be discussed in detail in the following:

1. Mesoscopic shape fluctuations in aligned multi lamellar stacks of DMPC (1,2-dimyristoyl-sn-glycero-3-phosphatidylcholine) bilayers were studied using the neutron spin-echo technique. From the dispersion relation in the fluid phase, values for the bilayer bending rigidity κ , the compressional modulus of the stacks B , and the effective sliding viscosity η_3 could be determined. This technique offers a novel approach to quantify the elasticity parameters in membranes by direct measurement of dynamical properties and also the impact of collective molecular motions on membrane properties [14].
2. Very recently, interprotein motions in a carboxymyoglobin protein crystal were reported from a molecular dynamics simulation [Phys. Rev. Lett. 100, 138102 (2008)]. Experimental evidence for a cooperative long range protein-protein interaction in purple membrane (PM) was found by inelastic neutron scattering. The dynamics was quantified by measuring the spectrum of the acoustic phonons in the 2d Bacteriorhodopsin (BR) protein lattice. The data were compared to an analytical model and the effective spring constant for the interaction between protein trimers was determined to be $k = 53.49$ N/m. The experimental results are in very good agreement to the computer simulations, which reported an interaction energy of 1 meV [15]. In this case, inelastic neutron scattering was used to study interactions between constituents

of a biological membrane.

Transport through membranes is one of the most fundamental functionalities of the bilayers [16, 17, 18, 19]. While transport channels or transport proteins are responsible for the transport of larger molecules, small molecules, such as water, can pass the bilayer with a certain probability. Despite the large body of experimental and theoretical work, it turns out to be very difficult to model the permeation of small molecules through bilayers on a microscopic level because of the large number of parameters involved. The solubility-diffusion model and the transient pore model are possible mechanisms for permeation of small molecules [18]: Pores seem to be the dominant permeation mechanism for ions for thin membranes. Ion permeation by partitioning and diffusion seems to become of greater importance as membrane thickness increases. Neutral molecules, such as water, cross by the solubility-diffusion mechanism because of their high solubility in the hydrocarbon phase. Recently Nagle *et al.* [20] and Mathai *et al.* [21] presented in a combined study the theoretical and experimental framework of a three layer theory for the passive permeability through bilayers. They link permeability to structural properties and strongly correlate it with the area per lipid, A , rather than with other structural quantities such as the thickness. Decades ago Träuble [22] (and later addressed by Marsh [23]) discussed the movement of molecules across membranes in terms of thermal fluctuations in the hydrocarbon chains of the membrane lipids. The thermal motion of the hydrocarbon chains results in the formation of conformational isomers, so-called kink-isomers of the hydrocarbon chains. "Kinks" may be pictured as mobile structural defects which represent small, mobile free volumes in the hydrocarbon phase of the membrane. The free volume needed for kink creation and movement might be created by propagating in-plane density fluctuations of the lipid acyl chains [24]. In a first inelastic neutron scattering experiment, the corresponding dispersion relation of the acyl tail dynamics in DMPC bilayers showed a drastic softening in the presence of ethanol molecules, which are known to increase bilayer permeability. Future experiments will elucidate the influence of ethanol on the collective dynamics in phospholipid bilayers.

II. COLLECTIVE VS. SINGLE-MOLECULE DYNAMICS

The spectrum of fluctuations in biomimetic and biological membranes covers a large range of time and length scales [2, 3, 8, 25, 26, 27, 28, 29, 30], ranging from the long wavelength

undulation and bending modes of the bilayer with typical relaxation times of nanoseconds and lateral length scales of several hundreds lipid molecules to the short wavelength density fluctuations in the picosecond range on nearest neighbor distances of lipid molecules. Local dynamics in lipid bilayers, i.e., dynamics of individual lipid molecules as vibration, rotation, libration (hindered rotation) and diffusion, have been investigated by, e.g., incoherent neutron scattering [25, 26, 27, 28, 29] and nuclear magnetic resonance [31, 32] to determine the short wavelength translational and rotational diffusion constant. Collective undulation modes have been investigated using neutron spin-echo spectrometers [14, 28, 29, 33] and dynamical light scattering [34, 35, 36].

Atomic and molecular motions in membranes can be classified as local, autocorrelated, and collective, pair correlated dynamics. Within the scattering formalism, autocorrelated dynamics is described by the incoherent scattering function, $S_{incoherent}(q, \omega)$, while the coherent scattering, $S_{coherent}(q, \omega)$, describes dynamics involving different molecules or atoms. Figure 2 exemplary depicts some of the local and collective modes in a phospholipid bilayer. Rotational and lateral diffusion, vibrations and rotations of the single lipid molecules can be investigated by e.g., incoherent inelastic neutron scattering, nuclear magnetic resonance or dielectric spectroscopy. On the other hand only coherent inelastic neutron scattering or inelastic x-ray scattering are able to elucidate the collective excitations such as, e.g., the short wavelength density fluctuations or undulation modes of the bilayer.

Experimentally, selective deuteration is used to emphasize the incoherent, respective coherent scattering over other contributions to the total sample scattering. While in protonated samples the incoherent scattering is normally dominant and the time-autocorrelation function of individual scatterers is accessible in neutron scattering experiments, (partial) deuteration emphasizes the coherent scattering and gives access to collective motions by probing the pair correlation function. Computer simulations offer direct access to incoherent and coherent properties by calculation of $S_{incoherent}(q, \omega)$ and $S_{coherent}(q, \omega)$ from the time evolution of atomic and molecular coordinates. Figure 3 visualizes some of the length and time scales involved for collective dynamics and the corresponding functional aspects. While permeability of bilayers occurs on distances of neighboring lipid molecules, elasticity might involve hundreds of membrane molecules. Coherent intra-protein dynamics will most likely be faster than inter-protein dynamics, which involves larger distances and in most cases a lipid mediated, elastic interaction.

III. EXPERIMENTAL

Only recently, the first inelastic scattering experiments in phospholipid bilayers to determine collective motions of the lipid acyl chains and in particular the short wavelength dispersion relation have been performed using inelastic X-ray [37] and neutron [24] scattering techniques. Note that only scattering experiments give wave vector resolved access to dynamical properties, what is important to associate excitation frequencies and relaxation times with specific molecular components and motions. In the case of single membranes the scattering signal is usually not sufficient for a quantitative study of the inelastic scattering. To maximize the scattering signal, multi lamellar samples composed of stacks of several thousands of lipid bilayers separated by layers of water, resulting in a structure of smectic A symmetry, were prepared. The high orientational order of the samples which gives rise to pronounced Bragg peaks and excitations is a prerequisite to a proper analysis of the corresponding correlation functions. Highly oriented multi lamellar membrane stacks of several thousands of lipid bilayers were prepared by spreading lipid solution of typically 25 mg/ml lipid in trifluoroethylene/chloroform (1:1) on 2" silicon wafers. About twenty such wafers separated by small air gaps were combined and aligned with respect to each other to create a "sandwich sample" consisting of several thousands of highly oriented lipid bilayers with a total mosaicity about 0.5°), and a total mass of about 400 mg of deuterated DMPC. The mosaicity of the sandwich is composed of the alignment of the bilayers within the stack on one wafer and of the orientation of different wafers with respect to each other. The use of well oriented samples leads to well localized elastic and inelastic signal in reciprocal space and allows to distinguish motions in the plane of the membranes ($q_{||}$) and perpendicular to the bilayers (q_z). During the experiments, the membranes were kept in a "Humidity Chamber" to control temperature and humidity and hydrated with D_2O from the vapor phase. The collective motions of the lipid acyl chains have been emphasized over other contributions to the inelastic scattering signal by using partially, chain deuterated lipids (DMPC -d54). The experiments that will be discussed here, were conducted on two different types of neutron spectrometers, namely triple-axis and spin-echo spectrometers. The accessible length and time scales of these spectrometers are discussed in more detail in Ref. [1]. The present paper focuses on the dynamics-property and dynamics-function aspects of the experiments.

A. Spin-echo Spectrometry

Fluctuations on the mesoscopic scale are determined by the elasticity parameters of the bilayers, i.e., the compressibility of the stacked membranes, B , and the bending modulus κ . The relaxations in this regime are in the nano-second time-range with accompanying small q -values. Spin-echo spectrometers turned out to be highly suited for these experiments. The spin-echo technique offers extremely high energy resolution from Larmor tagging the neutrons. A neutron spin echo measurement is in essence a measurement of neutron polarization [38]. A polarized neutron beam passes through a magnetic field perpendicular to the neutron polarization. The neutron spin precesses before arriving at the sample, acquiring a precession angle φ_1 . At the sample, the beam is scattered before passing through a second arm, acquiring an additional precession angle φ_2 in the reversed sense. For elastic scattering the total precession angle is $\Delta\varphi = \varphi_1 - \varphi_2 = 0$ for all incoming neutron velocities. If the neutron scatters inelastically by a small energy transfer $\hbar\omega$, there will be a linear change $\Delta\varphi = \tau \cdot \omega$ with τ being a real time in the case of quasielastic scattering. The spin-echo technique thus works in the time domain and measures the intermediate scattering function $S(q_{\parallel}, t)$ in contrast to the three-axis technique. For a quasielastic response, assumed to have Lorentzian lineshape with half-width Γ , the polarization will then show a single exponential decay $\text{PNSE} = P_s e^{-\Gamma t}$.

B. Triple-axis spectrometry

Fast motions in the ps time range due to sound propagation in the plane of the bilayer are best measured on triple-axis spectrometers. The energy of the incident and scattered neutrons is determined by Bragg scattering from crystal monochromators, (graphite in most cases). Advantages of triple-axis spectrometers are their relatively simple design and operation and the efficient use of the incoming neutron flux to the examination of particular points in (q, ω) space. By varying the three axes of the instrument, the axes of rotation of the monochromator, the sample and the analyzer, the wave vectors k_i and k_f and the energies E_i and E_f of the incident and the scattered neutrons, respectively, can be determined. The momentum transfer to the sample, and the energy transfer, $\hbar\omega$, are then defined by the laws of momentum and energy conservation to $q = k_f - k_i$ and $\hbar\omega = E_i - E_f$. The accessible

(q, ω) range is just limited by the range of incident neutron energies offered by the neutron guide as well as by mechanical restrictions of the spectrometer.

IV. ELASTIC PROPERTIES

According to linear smectic elasticity theory [39, 40] thermal fluctuations in the fluid phase of the membrane are governed by the free energy functional (Hamiltonian) [39, 40, 41]:

$$H = \int_A d^2r \sum_{n=1}^{N-1} \left(\frac{1}{2} \frac{B}{d} (u_{n+1} - u_n)^2 + \frac{1}{2} \kappa (\nabla_{\parallel}^2 u_n)^2 \right), \quad (1)$$

where κ denotes the bilayer bending rigidity, A the area in the xy -plane, N the number of bilayers, and u_n the deviation from the average position $n d$ of the n -th bilayer, d is the lamellar spacing. B and $K = \kappa/d$ are elastic coefficients, governing the compressional and bending modes of the smectic phase, respectively. A fundamental length scale in these systems is given by the smectic penetration length $\Lambda = \sqrt{K/B}$. Aligned lipid bilayers allow a separate determination of both parameters K and B [42, 43].

The spin-echo experiments were carried out at the IN11 and IN15 spectrometers, at the cold source of the high flux reactor of the Institut Laue-Langevin (ILL) in Grenoble, France. Wavelength bands centered at $\lambda=7.4\text{\AA}$ and $\lambda=14\text{\AA}$ with $\Delta\lambda/\lambda \simeq 0.15$ (FWHM), respectively, have been set by a velocity selector. The intermediate scattering function $S(q_{\parallel}, t)$ was measured for spin-echo times of $0.001\text{ns} < t < 20\text{ns}$ for IN11 and $0.01\text{ns} < t < 200\text{ns}$ for IN15. Data have been taken at three different temperatures, at 19°C , in the gel (ripple, $P_{\beta'}$) phase of the phospholipid bilayers, at 22°C , just above the temperature of the main transition in deuterated DMPC-d54 (at $T_m \approx 21.5^{\circ}\text{C}$), and at 30°C , far in the fluid L_{α} phase of the membranes and above the regime of so-called anomalous swelling. The corresponding lamellar d spacings were $d=56\text{\AA}$, 60\AA and 54\AA (gel, 22°C and fluid), respectively. Two relaxation processes, one at about 10 ns (τ_1) and a second, slower process at about 100 ns (τ_2) were observed. The relaxation rates τ_1^{-1} and τ_2^{-1} in the gel and the fluid phase are depicted in Fig. 4 (a) and (b). Both relaxation branches are dispersive. The fast process shows a q_{\parallel}^2 increase at small q_{\parallel} values and a bend at about $q_{\parallel} \approx 0.015\text{\AA}^{-1}$. The dispersion in the gel phase and close to the phase transition in Fig. 4 (b) appear to be more pronounced as compared to 30°C dispersion. A soft mode appeared in the $T=22^{\circ}\text{C}$ dispersion, indicating a significant softening of the bilayer at a well defined wave number. The slow branches at

T=19°C and 30°C also show increasing relaxation rates with increasing $q_{||}$ values, but with a distinct non-polynomial behavior.

The dispersion relation of the fast branch with relaxation rates between 1 and 10 ns can be attributed to undulation dynamics. Qualitatively, at very small $q_{||}$ -values, the membranes behave as liquid films and their dynamics is basically determined by the viscosity of the water layer in between the stacked membranes (*film regime*). With increasing $q_{||}$ there is a transition into a *bulk-elasticity* regime where the dynamics depends on the elastic properties of the lipid bilayers. At this point, the dispersion bifurcates in two relaxation branches. The faster one, which is out the experimentally accessible time window of the spin-echo spectrometer, is mainly determined by the compressional modulus B . The slower one, which is observed here, can be assigned to the bending modulus κ . The slow dispersion branch with relaxation rates of about 100 ns could be attributed to a surface relaxation mode [44, 45], which is particular to a stack of membranes.

Following the idea of Ribotta [13], the relaxation rates of the undulations can be described by:

$$\tau^{-1}(q_{||}) = \frac{\kappa/d}{\eta_3} q_{||}^2 \frac{q_{||}^4 + (\pi/(\Lambda D))^2}{q_{||}^4 + \frac{1}{\mu\eta_3}(\pi/D)^2} \quad (2)$$

(η_3 is the layer sliding viscosity), and following results were obtained: $\kappa = 14.8 \pm 8k_B T$, $\Lambda = 10.3 \pm 2.3 \text{ \AA}$, $\eta_3 = 0.016 \pm 0.0006 \text{ Pa s}$. B was calculated to $B=1.08 \cdot 10^7 \text{ J/m}^3$ ($d=54 \text{ \AA}$). These values agree quite well with values reported in the literature [30, 46, 47, 48]. The resulting effective sliding viscosity of the membrane system η_3 was found to be 16 times higher than that of water, what points to different properties of the interstitial hydration water, as compared to bulk water. Note that Eq. 2 does not describe a pure undulation mode, which is probed at q_z values of $q_z = 2\pi/d$, only. If the scattering is probed at finite components $\delta q_z := (q_z - 2\pi/d)$ or measured with a relaxed q_z resolution, there is a mixing of *baroclinic* modes, which are distinctly slower than a pure undulation because they involve a relocation motion of the water layer. The parameter D describes an effective finite-size cutoff-length, which was related to the instrumental resolution $D = \pi/\Delta q_z$.

From the soft-mode in the fluid dispersion, it seems that the well known softening of phospholipid membrane upon approaching the main phase transition temperature from the fluid phase, i.e., the regime of "critical swelling" or "anomalous swelling" [48], occurs on a well defined length scale, only ($2\pi/q_{||} \approx 420 \text{ \AA}$). Using atomic force microscopy (AFM),

pronounced ripples were observed in the $P_{\beta'}$ phase of stacked membranes, with an increasing ripple periodicity Λ_r when approaching the temperature of the main transition at $T_m = 24\text{ }^\circ\text{C}$ [49]. Close to T_m , coexisting metastable ripples with $2\Lambda_r \approx 420\text{ \AA}$ were observed. The experiments therefore point to coexisting *nanodomains* with sizes of less than 50 nm in the range of *critical swelling* [50, 51, 52] of phospholipid bilayers. The existence of coexisting small gel and fluid domains has also been argued by preceding AFM investigations [53, 54] to compensate the large stress which occurs at T_m due to the volume difference of the two phases. The softening in the range of the phase transition is most likely coupled to the occurrence of these metastable $2\Lambda_r$ ripples. Bending of the bilayers might occur mainly in the interfaces between two metastable ripples where the bending modulus can be expected to be softer because structure and interactions are likely to be much less well defined in the interface. Not much energy would be needed to slightly change the tilt angle between to ripple flanks. Note that the relation between critical swelling and softening of the bilayers, and the formation of a low temperature ripple phase is not trivial [52, 55] and the anomalous swelling is not directly coupled to the formation of ripples. Inelastic experiments in different systems are definitely needed to better understand the impact of the soft-mode in the DMPC dispersion curve. The most important contribution of the NSE technique is that the 'stiffness' of the bilayers is determined as a function of internal length scale. It seems that there is no global softening, but softening occurs on of certain length scales, only.

V. COLLECTIVE PROTEIN INTERACTION

The high protein concentration in biological membranes might lead to long-range protein-protein interactions, on which there have been speculations, already some time ago [2]. Recently, interprotein motions in a carboxymyoglobin protein crystal were reported from a molecular dynamics simulation [56, 57]. Motions in proteins occur on various length and time scales [6, 7], and the functional behavior of membrane proteins is likely to depend on the lipid bilayer composition and physical properties, such as hydrophobic thickness and elastic moduli. How the variety of inter- and intra-protein motions, occurring over different time and length scales, interact to result in a functioning biological system remains an open field for those working at the interface of physics and biology. Purple Membrane (PM) occurs naturally in the form of a two-dimensional crystal, consisting of 75% (wt/wt) of a

single protein, Bacteriorhodopsin (BR), that functions as a light-activated proton pump, and 25% various lipid species (mostly phospho- and glyco-lipids) [58]. BR is a proton transporting membrane protein, formed of seven trans-membrane alpha-helices arranged around the photosensitive retinal molecule. The protein in the lipid matrix is organized in trimers that form a highly ordered 2d hexagonal lattice with lattice parameter $a \approx 62 \text{ \AA}$, as depicted in Fig. 5 (a).

The experiments were performed on the IN12 cold-triple-axis spectrometer at the Institut Laue Langevin (Grenoble, France). It allows the measurement of diffraction and inelastic scattering in the same run without changing the set-up, which is crucial to assign dynamical modes to structural properties and molecular components. Correlations and motions in membranes are often well separated in reciprocal space because of the largely different length and time scales involved. The prominent distances in PM, such as lipid–lipid and BR–BR monomers and trimers for instance lead to spatially well separated signals. The same holds for the different time scales involved from the picosecond (molecular reorientations) to the nano- or microsecond (membrane undulations, large protein motions). The use of oriented samples further allows to separate correlations in the plane of the membranes, and perpendicular to the bilayers. Dynamics between different protein trimers is expected to be dominant where the 2d BR diffraction pattern is observed, i.e., in a q_{\parallel} range of about 0.1 \AA^{-1} to 0.6 \AA^{-1} .

The excitation spectrum of the 2d protein lattice was modeled analytically, taking the protein trimers as the centers of a primitive hexagonal lattice with lattice constant $a = 62 \text{ \AA}$. The model is depicted in Fig. 5(a). The basic hexagonal translations are marked by arrows. The interaction between the protein trimers is contained in springs with an effective (longitudinal) spring constant k (Fig. 5(b)). The calculated $C_l(q, \omega)$ is shown in Fig. 6(b). The statistical average leads to a superposition of the different phonon branches, which start and end in the hexagonal Bragg peaks (at $\hbar\omega = 0$). The absolute phonon energies can not be determined from the model, but depend on the coupling constant k . So the energy of the phonon curves in Fig. 6(b) was scaled to match the experiment. Note that because the proteins trimers were treated as dots with an effective mass of M_{tr} , the calculation does not include any contributions from intra-protein or intra-trimer dynamics, i.e., possible optical modes and phonons. The longitudinal phonon spectrum $C_l(q, \omega) = (\omega^2/q^2)S(q, \omega)$ for q_{\parallel} values between 0.34 \AA^{-1} and 0.46 \AA^{-1} is shown in Figure 6(a). The most pronounced

phonon branches from Figure 6(b) were plotted as solid lines in part (a) for comparison. In the q_{\parallel} range between 0.34 \AA^{-1} and about 0.43 \AA^{-1} , the experiment well reproduces the calculated phonon curves. The agreement is less good for q_{\parallel} values above 0.43 \AA^{-1} . Only the strongest phonon branches are visible in the data, the weaker branches can most likely not be resolved from the background.

Experiment and calculation can be compared to the MD simulations in Ref. [56], where a peak in the energy spectrum at 1 meV was identified as a translational intermolecular protein:protein interaction vibration in a carboxymyoglobin protein crystal. The energy agrees well with the energy of the zone boundary phonon in PM of 1.02 meV, as shown in Fig. 6. The good agreement of the energy values in the two systems most likely stems from the very high protein density in PM, which makes it almost crystal like. The computational work thus strongly supports the interpretation of our data as collective protein:protein excitations. The commonly assumed interaction mechanism between inclusions in membranes is a lipid-mediated interaction due to local distortions of the lipid bilayer [59, 60, 61, 62, 63], with a strong dependence on the bilayer properties, in particular elastic properties. The PM might, however, be a special case because there are very few lipids between neighboring BR proteins [64]. While the nature of the interaction still will be mainly elastic, it is not likely to be purely lipid-mediated but for the most part a direct protein-protein interaction. The strength of the interaction can be determined from the data in Fig. 6. The energy of the zone-boundary phonon at the M-point of the hexagonal Brillouin zone (for instance at a q_{\parallel} value of 0.35 \AA^{-1}) relates to the coupling constant by $M_{tr}\omega^2 = 6k$. Because this energy is determined as $\hbar\omega = 1.02 \text{ meV}$, the effective protein-protein spring constant k is calculated to $k = 53.49 \text{ N/m}$ [66]. On the microscopic level, displacing the BR trimer by 1 \AA yields a force between neighboring trimers of 5.3 nN. There is therefore strong protein-protein communication in PM. Using the same approach, the spring constant for graphite for comparison is calculated to 27,000 N/m for the in-plane interaction, and 3.5 N/m for out-of-plane interactions. The force constant that we measure in PM thus is 1-2 orders of magnitude larger than the effective van-der-Waals force constant in graphite, but 2-3 orders of magnitude weaker than a C-C bond.

VI. CONCLUSION

Inelastic scattering experiments give access to molecular dynamics and correlations in membranes. The experiments prove that relevant properties and functional aspects of the bilayers can be quantified from coherent dynamics. Future experiments will allow to study intra and inter protein dynamics of membrane embedded proteins and how bilayer composition and physical properties affect protein function. Membranes with specific properties might be tailored for specific applications and protein function of membrane embedded proteins might be enhanced (or suppressed) by adapting the properties of the surrounding bilayer.

Acknowledgement: It is my pleasure to thank Christoph Ollinger, Giovanna Fragneto, Franz Demmel, Wolfgang Häußler, Karin Schmalzl, Kathleen Wood, Dieter Strauch, who were involved in the original work, and in particular Tim Salditt for his continuous support and a very fruitful collaboration. The Institut Laue-Langevin provided ample beam time to conduct the experiments.

-
- [1] M. C. Rheinstädter, T. Seydel, W. Häußler, and T. Salditt, *J. Vac. Sci. Technol. A* **24**, 1191 (2006).
- [2] R. Lipowsky and E. Sackmann, eds., *Structure and Dynamics of Membranes*, vol. 1 of *Handbook of Biological Physics* (Elsevier, Amsterdam, 1995).
- [3] T. Salditt, *Curr. Opin. Colloid Interface Sci.* **5**, 19 (2000).
- [4] S. Krueger, *Curr. Opin. Coll. Inter. Scie.* **6**, 111 (2001).
- [5] T. Salditt, *J. Phys.: Condens. Matter* **17**, R287R314 (2005).
- [6] H. Frauenfelder, S. Sligar, and P. Wolynes, *Science* **254**, 15981603 (1991).
- [7] P. Fenimore, H. Frauenfelder, B. McMahon, and R. Young, *Proc. Natl. Acad. Sci. U.S.A.* **101**, 1440814413 (2004).
- [8] T. Bayerl, *Curr. Opin. Colloid Interface Sci.* **5**, 232 (2000).
- [9] M. Tarek, D. Tobias, S.-H. Chen, and M. Klein, *Phys. Rev. Lett.* **87**, 238101 (4 pages) (2001).
- [10] J. S. Hub, T. Salditt, M. C. Rheinstädter, and B. L. de Groot, *Biophysical J.* **93**, 3156 (2007).
- [11] P. de Gennes, *The Physics of Liquid Crystals* (Clarendon Press, Oxford, 1974).
- [12] E. Kats, V. Lebedev, and A. Muratov, *Phys. Rep.* **228**, 1 (1993).
- [13] R. Ribotta, D. Salin, and G. Durand, *Phys. Rev. Lett.* **32**, 6 (1974).
- [14] M. C. Rheinstädter, W. Häußler, and T. Salditt, *Phys. Rev. Lett.* **97**, 048103 (4 pages) (2006).
- [15] M. C. Rheinstadter, K. Schmalzl, K. Wood, and D. Strauch (2008), <http://arxiv.org/abs/0803.0959>.
- [16] D. Huster, J. Jin, Albert, K. Arnold, and K. Gawrisch, *Biophys. J.* **73**, 855 (1997).
- [17] B. Deamer and J. Bramhall, *Chem. Phys. Lipids* **40**, 167 (1986).
- [18] S. Paula, A. Volkov, A. Van Hoek, T. Haines, and D. Deamer, *Biophys. J.* **70**, 339 (1996).
- [19] G. Lahajnar, P. Macek, P. Smid, and I. Zupancic, *Biochim Biophys Acta.* **1235**, 437 (1995).
- [20] J. F. Nagle, J. C. Mathai, M. L. Zeidel, and S. Tristram-Nagle, *J. Gen. Physiol.* **131**, 77 (2008).
- [21] J. C. Mathai, S. Tristram-Nagle, J. F. Nagle, and M. L. Zeidel, *J. Gen. Physiol.* **131**, 69 76 (2008).
- [22] H. Träuble, *J. Membrane Biol.* **4**, 193 (1971).
- [23] D. Marsh, *J. Membrane Biol.* **18**, 145 (1974).

- [24] M. C. Rheinstädter, C. Ollinger, G. Fragneto, F. Demmel, and T. Salditt, *Phys. Rev. Lett.* **93**, 108107 (4 pages) (2004).
- [25] S. König, W. Pfeiffer, T. Bayerl, D. Richter, and E. Sackmann, *J. Phys. II France* **2**, 1589 (1992).
- [26] S. König, E. Sackmann, D. Richter, R. Zorn, C. Carlile, and T. Bayerl, *J. Chem. Phys.* **100**, 3307 (1994).
- [27] S. König, T. Bayerl, G. Coddens, D. Richter, and E. Sackmann, *Biophys. J.* **68**, 1871 (1995).
- [28] W. Pfeiffer, T. Henkel, E. Sackmann, and W. Knorr, *Europhys. Lett.* **8**, 201 (1989).
- [29] W. Pfeiffer, S. König, J. Legrand, T. Bayerl, D. Richter, and E. Sackmann, *Europhys. Lett.* **23**, 457 (1993).
- [30] E. Lindahl and O. Edholm, *Biophys. J.* **79**, 426 (2000).
- [31] A. Nevzorov and M. Brown, *J. Chem. Phys.* **107**, 10288 (1997).
- [32] M. Bloom and T. Bayerl, *Can. J. Phys.* **73**, 687 (1995).
- [33] T. Takeda, Y. Kawabata, H. Seto, S. Komura, S. Gosh, M. Nagao, and D. Okuhara, *J. Phys. Chem. Solids* **60**, 1375 (1999).
- [34] R. Hirn, T. Bayerl, J. Rädler, and E. Sackmann, *Faraday Discuss.* **111**, 17 (1999).
- [35] R. B. Hirn and T. M. Bayerl, *Phys. Rev. E* **59**, 5987 (1999).
- [36] M. F. Hildenbrand and T. M. Bayerl, *Biophys. J.* **88**, 3360 (2005).
- [37] S. Chen, C. Liao, H. Huang, T. Weiss, M. Bellisent-Funel, and F. Sette, *Phys. Rev. Lett.* **86**, 740 (2001).
- [38] F. Mezei, ed., *Neutron Spin Echo* (Springer, Berlin, 1980).
- [39] A. Caillé, *C.R. Acad. Sci. Ser. B* **274**, 891 (1972).
- [40] N. Lei, C. Safinya, and R. Bruinsma, *J. Phys. II* **5**, 1155 (1995).
- [41] N. Lei, Ph.D. Dissertation, Rutgers (1993).
- [42] Y. Lyatskaya, Y. Liu, S. Tristram-Nagle, J. Katsaras, and J. F. Nagle, *Phys. Rev. E* **63**, 011907 (9 pages) (2001).
- [43] T. Salditt, M. Vogel, and W. Fenzl, *Phys. Rev. Lett.* **90**, 178101 (4 pages) (2003).
- [44] H. Bary-Soroker and H. Diamant, *Europhys. Lett.* **73**, 871 (2006).
- [45] H. Bary-Soroker and H. Diamant, *Phys. Rev. E* **76**, 042401 (4 pages) (2007).
- [46] C. Ollinger, D. Constantin, J. Seeger, and T. Salditt, *Europhys. Lett.* **71**, 311 (2005).
- [47] H. I. Petrache, N. Gouliaev, S. Tristram-Nagle, R. Zhang, R. M. Suter, and J. F. Nagle, *Phys.*

- Rev. E **57**, 7014 (1998).
- [48] G. Pabst, J. Katsaras, V. A. Raghunathan, and M. Rappolt, *Langmuir* **19**, 1716 (2003).
- [49] A. Schäfer, T. Salditt, and M. C. Rheinstädter, *Phys. Rev. E* **77**, 021905 (8 pages) (2008).
- [50] F. Chen, W. Hung, and H. Huang, *Phys. Rev. Lett.* **79**, 4026 (1997).
- [51] J. Nagle, H. Petrache, N. Gouliarov, S. Tristram-Nagle, Y. Liu, R. Suter, and K. Gawrisch, *Phys. Rev. E* **58**, 7769 (1998).
- [52] P. Mason, J. Nagle, R. Eppand, and J. Katsaras, *Phys. Rev. E* **63**, 030902(R) (4 pages) (2001).
- [53] A. F. Xie, R. Yamada, A. A. Gewirth, and S. Granick, *Phys. Rev. Lett.* **89**, 246103 (4 pages) (2002).
- [54] F. Tokumasu, A. Jin, and A. Dvorak, *J. Electron Microsc.* **51**, 1 (2002).
- [55] G. Pabst, H. Amenitsch, D. Kharakoz, P. Laggnier, and M. Rappolt, *Phys. Rev. E* **70**, 021908 (9 pages) (2004).
- [56] V. Kurkal-Siebert, R. Agarwal, and J. C. Smith, *Phys. Rev. Lett.* **100**, 138102 (4 pages) (2008).
- [57] L. Meinhold, J. C. Smith, A. Kitao, and A. H. Zewail, *Proc. Natl. Acad. Sci. U.S.A.* **104**, 17261 (2007).
- [58] U. Haupts, J. Tittor, and D. Oesterhelt, *Annu. Rev. Biophys. Biomol. Struct.* **28**, 367 (1999).
- [59] P. A. Kralchevsky, *Adv. Biophys.* **34**, 25 (1997).
- [60] K. Bohinc, V. Kralj-Iglič, and S. May, *J. Chem. Phys.* **119**, 7435 (2003).
- [61] P. Biscari and F. Bisi, *Eur. Phys. J. E* **6**, 381 (2002).
- [62] P. Lagüe, M. J. Zuckermann, and B. Roux, *Biophys. J.* **81**, 276 (2001).
- [63] N. Dan, P. Pincus, and S. Safran, *Langmuir* **9**, 2768 (1993).
- [64] J. Baudry, E. Tajkhorshid, F. Molnar, J. Phillips, and K. Schulten, *J. Phys. Chem.* **105**, 905 (2001).
- [65] J. F. Hunt, P. D. McCrea, G. Zaccai, and D. M. Engelman, *J. Mol. Biol.* **273**, 1004 (1997).
- [66] The molecular weight of a BR monomer is 26.9 kDa [65]. Because $1 \text{ kg} = 6.0221 \times 10^{26} \text{ Dalton}$, the BR trimer thus weighs $m_{tr} = 1.34 \cdot 10^{-22} \text{ kg}$

Figure Legends

Figure 1

(Color online). Cartoon of a cell membrane. Courtesy of Mariana Ruiz Villarreal (http://commons.wikimedia.org/wiki/Image:Cell_membrane_detailed_diagram.svg).

Figure 2

(Color online). Some elementary dynamical modes in lipid bilayers. (a) Local modes include diffusion and vibrations, rotations and librations (hindered rotations) of single lipid molecules. (b) Collective excitations are coherent motions of several membrane molecules, such as the long wavelength undulation and bending modes of the membranes.

Figure 3

(Color online). Length and time scale for some collective motions and corresponding functional aspects. While permeability occurs on nearest neighbor distances of lipid molecules, membrane elasticity involves several hundreds of lipid molecules. Besides collective intra-protein dynamics, there might also be an interaction between different proteins in biological membranes, i.e., an inter-protein dynamics.

Figure 4

(Color online). (a) Dispersion relations at $T=30^\circ\text{C}$. The solid line is a fit to Eq. (2). (b) Dispersion relations in the gel (19°C) and in the fluid phase (22°C). A pronounced soft mode is observed at $q_0 \approx 0.015 \text{ \AA}^{-1}$ at 22°C (dotted vertical line). Solid lines in (b) are guides to the eye. (From [14].)

Figure 5

(Color online). (a) BR trimers are arranged on a hexagonal lattice of lattice constant $a \approx 62 \text{ \AA}$. (b) The interaction between the protein trimers is depicted as springs with

effective spring constant k . (From [15].)

Figure 6

(Color online). (a) Experimental $C_l(q, \omega)$, measured in the the third Brillouin zone. (b) Calculated excitation spectrum $C_l(q, \omega)$ in the range of the experimental data. The most strongest phonon branches are also shown in part (a) as solid lines. (From [15].)

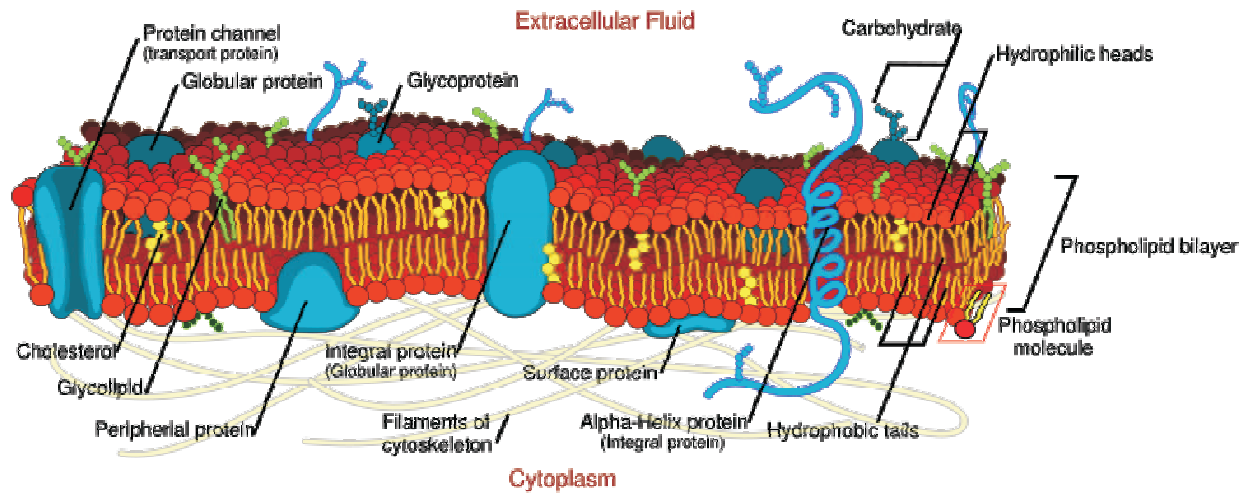


FIG. 1:

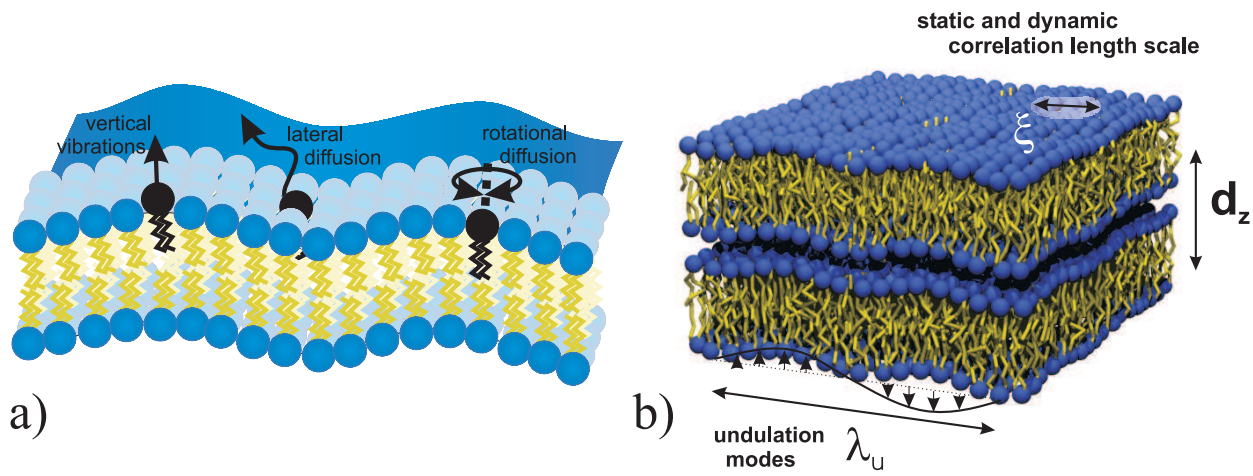


FIG. 2:

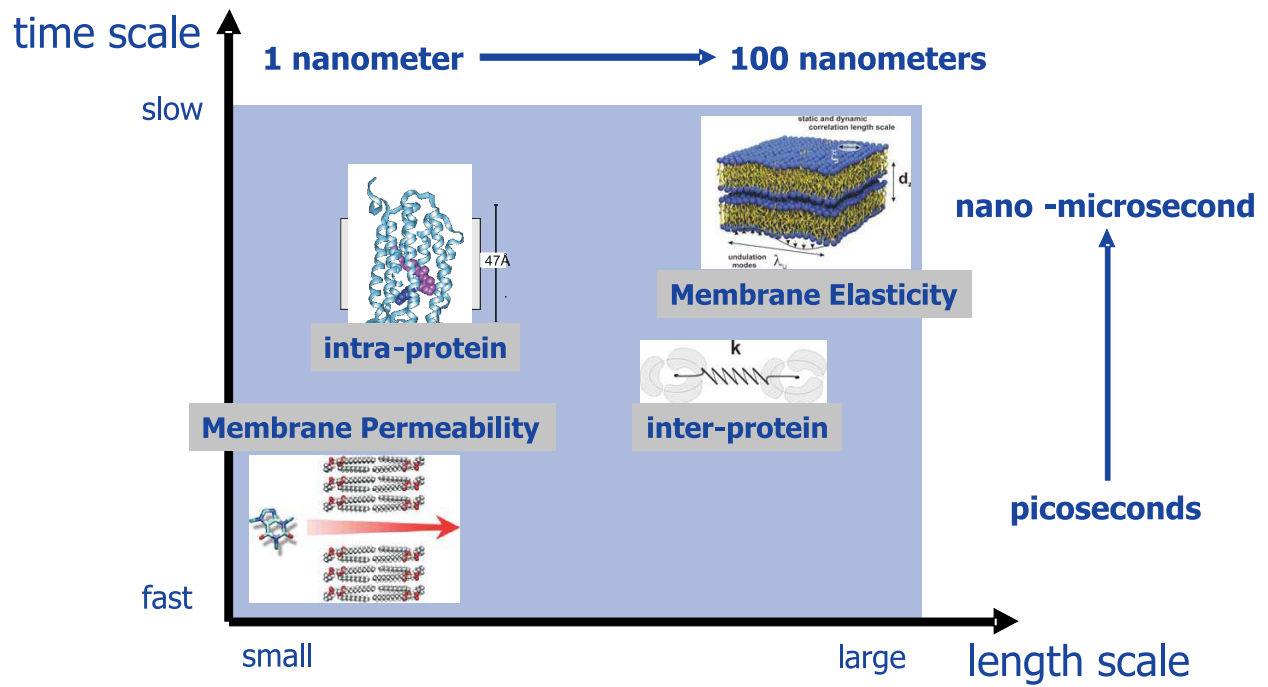


FIG. 3:

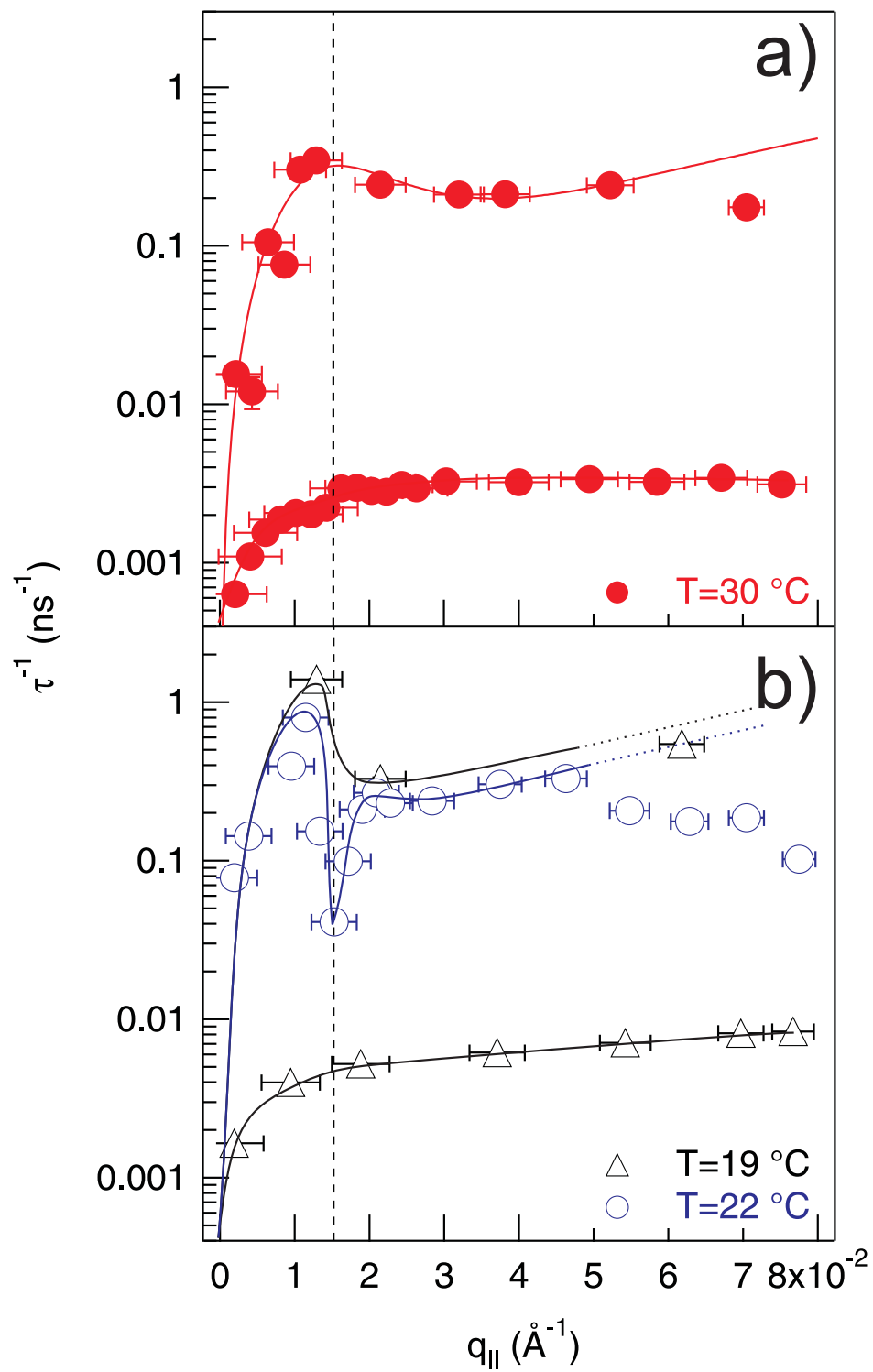


FIG. 4:

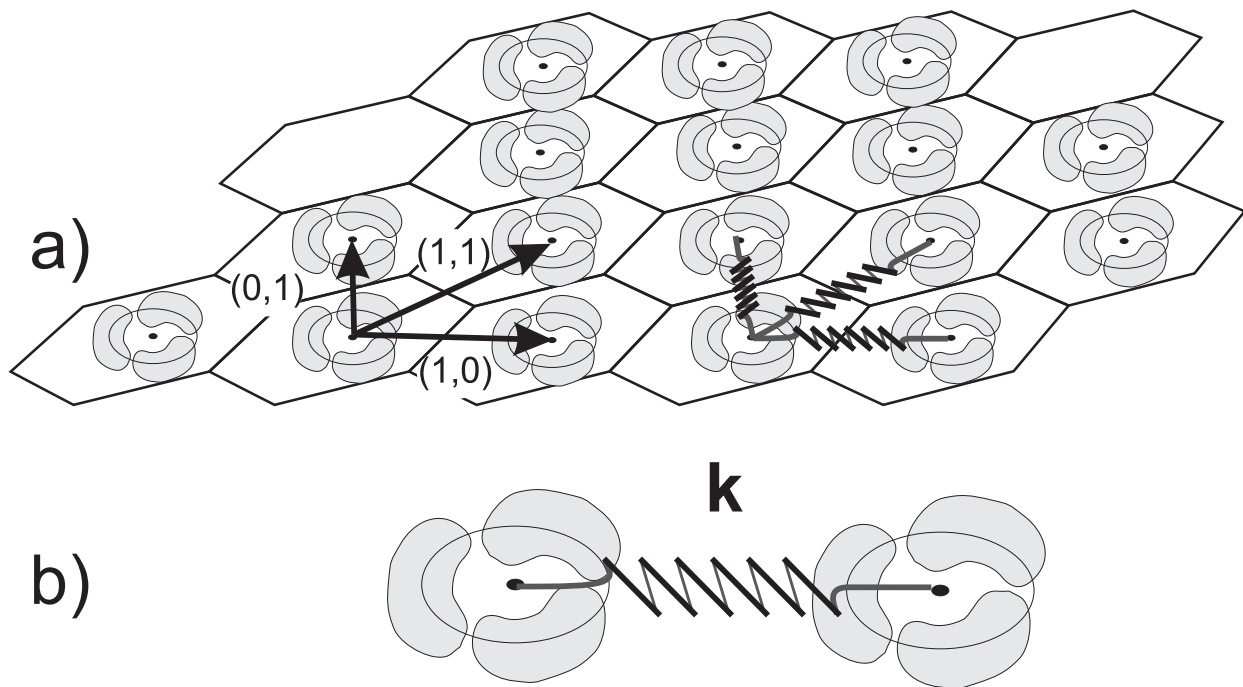


FIG. 5:

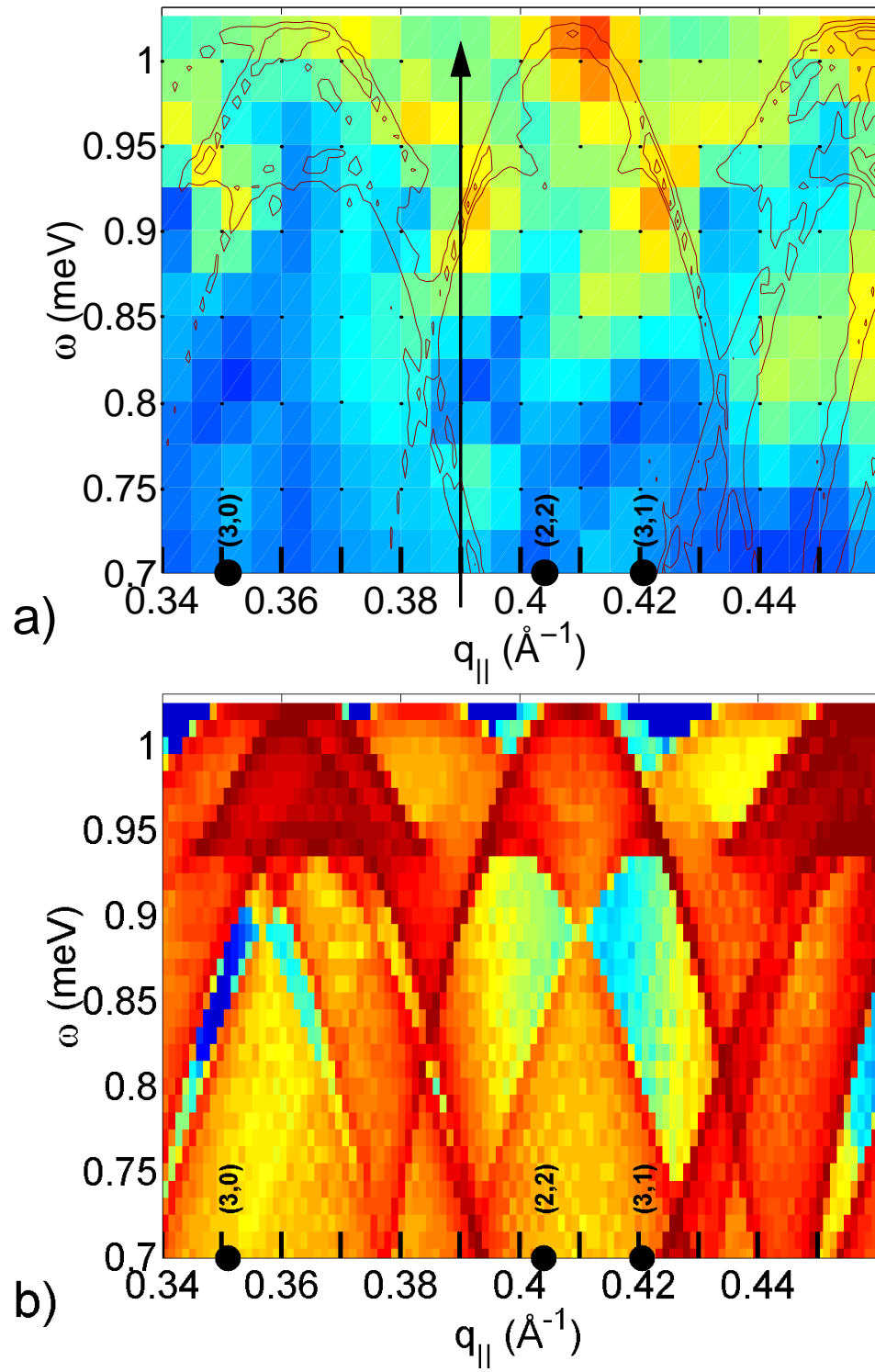


FIG. 6: